

COMPUTATION OF THREE-DIMENSIONAL MIXED CONVECTIVE  
BOUNDARY LAYER FLOW

Prashant Gadepalli and Muhammad M. Rahman  
Department of Mechanical Engineering  
University of South Florida  
Tampa, Florida

404561  
52-34  
45045  
p. 12

ABSTRACT

The paper presents the numerical solution of heat and mass transfer during cross-flow (orthogonal) mixed convection. In this class of flow, a buoyancy-driven transport in the vertical direction and a forced convective flow in the horizontal direction results in a three-dimensional boundary layer structure adjacent to the plate. The rates of heat and mass transfer are determined by a combined influence of the two transport processes. The equations for the conservation of mass, momentum, energy, and species concentration were solved along with appropriate boundary conditions to determine the distributions of velocity components, temperature, and concentration across the thickness of the boundary layer at different locations on the plate. Results were expressed in dimensionless form using Reynolds number, Richardson number for heat transfer, Richardson number for mass transfer, Prandtl number, and Schmidt number as parameters. It was found that the transport is dominated by buoyancy at smaller vertical locations and at larger distances away from the forced convection leading edge. Effects of forced convection appeared to be very strong at smaller horizontal distances from the leading edge. The cross-stream forced convection enhanced the rate of heat and mass transfer by a very significant amount.

INTRODUCTION

Heat and mass transfer under the combined influence of a vertical buoyant force and an externally-imposed horizontal flow occurs frequently in nature and has several technological applications as well. Some examples of such cross-flow mixed convection are: the cooling of electronic circuit boards by fans, heat transfer from vertical walls in buildings, heat loss mechanisms from solar collectors, mass transfer during a drying process, and wind-driven propagation of fire.

There have been a number of past studies devoted to the understanding of mixed convective heat and mass transfer. These include aiding, opposing, and cross flow situations. Lin et al. (ref.1) have studied the mixed convection problem of an isothermal horizontal plate moving in parallel or reversely to a free stream. They concluded that the heat transfer rate increases significantly with increase in buoyancy, and increase in the velocities of the plate and the free stream. Khouaja et al. (ref.2) studied mixed convection in slender vertical cylinders for power law variation in surface heat flux. They found that the local heat transfer rate increases with increasing Prandtl number, increasing curvature, and increasing value of power law exponent. A vertical flat plate was simulated as a limiting form of the cylinder and provided satisfactory results. Wickern (ref.3) studied mixed convection from an arbitrarily inclined semi-infinite flat plate for different inclination angles and for different Prandtl numbers. He found that for opposing buoyancy forces, singular as well as regular behavior can occur.

In a cross-flow situation, the transport is more complicated because of the three-dimensional nature of the boundary layer flow. In an early study, Young and Yang (ref.4) used a perturbation analysis and found that a weak cross-flow has very little effect on natural convection over a vertical flat surface. Eichorn and Hasan (ref.5) as well as Plumb (ref.6) have obtained similarity solutions for Falkner-Skan type three-dimensional mixed convection. But similarity exists only for certain power law surface

temperature distributions. Evans and Plumb (refs. 7, 8) extended the box scheme developed by Keller and Cebeci (ref.9) to three dimensions and obtained numerical solutions for mixed convection from an isothermal surface in a cross-flow. Rahman and Carey (refs. 10,11) examined the transient behavior of the flow that may precede the final steady state configuration. They looked at heat transfer from a vertical plate in a number of transient conditions. They found that under certain conditions, the local velocity and temperature fields overshoot before reaching the final steady-state configuration.

The present study explored the process of combined heat and mass transfer during cross-flow mixed convection. The three-dimensional cross-flow boundary layer flow was analyzed when buoyancy-driven flow and transport in the vertical direction was the same order of magnitude as the forced convection in the horizontal direction. Equations governing the conservation of mass, momentum, energy, and species concentration were solved numerically to predict velocity, temperature, and concentration distribution across the boundary layer and the variation of heat and mass transfer rate over the plate. A parametric study was performed to determine the effects of Reynolds, Richardson ( $Ri$  and  $Ri^*$ ), Prandtl, and Schmidt numbers.

### MATHEMATICAL MODEL

The schematic of the problem under consideration is shown in Figure 1. A vertical flat plate of finite length and height is placed in an extensive horizontal fluid stream. The surface of the plate is maintained at a constant temperature  $T_0$  and the concentration of the diffusing medium at the surface remains constant at  $C_0$ . The ambient fluid is at a constant temperature  $T_\infty$  and has the diffusing species with a constant concentration  $C_\infty$ . It is assumed that  $T_0 > T_\infty$  and  $C_0 > C_\infty$ . The velocity of the fluid in the free stream far away from the plate remains constant at  $w_\infty$ . A three-dimensional boundary layer flow develops adjacent to the plate due to the combined effects of the horizontal forced flow and buoyancy force due to temperature and concentration differences acting in the vertical direction. The characteristics of the mixed convective flow are determined by the relative magnitudes of the forced and buoyancy-driven flows.

The equations describing the conservation of mass, momentum, energy, and concentration inside the boundary layer for steady, incompressible, laminar flow, with constant fluid properties (Boussinesq approximation for buoyancy) are given by:

$$\frac{\partial u}{\partial x} + \frac{\partial v}{\partial y} + \frac{\partial w}{\partial z} = 0 \quad (1)$$

$$u \frac{\partial u}{\partial x} + v \frac{\partial u}{\partial y} + w \frac{\partial u}{\partial z} = \nu \frac{\partial^2 u}{\partial x^2} + g\beta (T - T_\infty) + g\beta^* (C - C_\infty) \quad (2)$$

$$u \frac{\partial w}{\partial x} + v \frac{\partial w}{\partial y} + w \frac{\partial w}{\partial z} = \nu \frac{\partial^2 w}{\partial x^2} \quad (3)$$

$$u \frac{\partial T}{\partial x} + v \frac{\partial T}{\partial y} + w \frac{\partial T}{\partial z} = \alpha \frac{\partial^2 T}{\partial x^2} \quad (4)$$

$$u \frac{\partial C}{\partial x} + v \frac{\partial C}{\partial y} + w \frac{\partial C}{\partial z} = D \frac{\partial^2 C}{\partial x^2} \quad (5)$$

The boundary conditions are given by:

$$x = 0 : v = 0, w = 0, T = T_0, C = C_0 \quad (6)$$

$$x \rightarrow \infty : v = 0, w = w_\infty, T = T_\infty, C = C_\infty \quad (7)$$

$$y = 0 : v = 0, w = w_\infty, T = T_\infty, C = C_\infty \quad (8)$$

$$z = 0 : v = 0, w = w_\infty, T = T_\infty, C = C_\infty \quad (9)$$

It is convenient to define the following non-dimensional variables at this point.

$$\theta = \frac{T - T_\infty}{T_0 - T_\infty} ; \quad \psi = \frac{C - C_\infty}{C_0 - C_\infty}$$

$$U = \frac{u}{w_\infty} , \quad V = \frac{v}{w_\infty} , \quad W = \frac{w}{w_\infty}$$

$$X = \frac{x}{L} , \quad Y = \frac{y}{L} , \quad Z = \frac{z}{L}$$

Using the above non-dimensionalized variables, the governing equations (1-5) can be expressed as:

$$\frac{\partial U}{\partial X} + \frac{\partial V}{\partial Y} + \frac{\partial W}{\partial Z} = 0 \quad (10)$$

$$U \frac{\partial V}{\partial X} + V \frac{\partial V}{\partial Y} + W \frac{\partial V}{\partial Z} = \frac{1}{Re} \frac{\partial^2 V}{\partial X^2} + Ri \theta + Ri \psi \quad (11)$$

$$U \frac{\partial W}{\partial X} + V \frac{\partial W}{\partial Y} + W \frac{\partial W}{\partial Z} = \frac{1}{Re} \frac{\partial^2 W}{\partial X^2} \quad (12)$$

$$U \frac{\partial \theta}{\partial X} + V \frac{\partial \theta}{\partial Y} + W \frac{\partial \theta}{\partial Z} = \frac{1}{Re \cdot Pr} \frac{\partial^2 \theta}{\partial X^2} \quad (13)$$

$$U \frac{\partial \psi}{\partial X} + V \frac{\partial \psi}{\partial Y} + W \frac{\partial \psi}{\partial Z} = \frac{1}{Re \cdot Sc} \frac{\partial^2 \psi}{\partial X^2} \quad (14)$$

And, the boundary conditions (6-10) are transformed to :

$$X = 0 : V = 0, \quad W = 0, \quad \theta = 1, \quad \psi = 1 \quad (15)$$

$$X \rightarrow \infty : V = 0, \quad W = 1, \quad \theta = 0, \quad \psi = 0 \quad (16)$$

$$Y = 0 : V = 0, \quad W = 1, \quad \theta = 0, \quad \psi = 0 \quad (17)$$

$$Z = 0 : V = 0, \quad W = 1, \quad \theta = 0, \quad \psi = 0 \quad (18)$$

The governing equations (10-14) contain the Reynolds number, Re, Prandtl number, Pr, Schmidt number, Sc, Richardson number, Ri, and Richardson number for mass transfer  $Ri^*$  as parameters. The relative magnitude of these parameters determines the characteristics of the flow. The effects of each of these parameters on the flow configuration has been studied during the course of the present investigation. The parameters were varied over the following range.  $Re = 10^3, 10^4, \text{ and } 10^5$ ;  $Pr = 0.7 \text{ and } 7$  (corresponding to air and water respectively);  $Sc = 0.6 \text{ and } 580$  (nominally for water vapor-air system and sodium chloride - water system);  $Ri = 1, 10, \text{ and } 100$ ; and  $Ri^* = 1, 10 \text{ and } 100$ .

## COMPUTATIONAL PROCEDURE

The governing transport equations, along with the boundary conditions described in the previous section were solved numerically using the PHOENICS computer program. A Cartesian grid structure covering the entire boundary layer region was used for the computation. The distribution of cells in the computation domain was determined from a series of test runs with different number of cells in the x, y, and z directions. It was found that  $60 \times 20 \times 20$  cells are adequate for the present computation. The finite volume equations were derived by using the principles of conservation of mass, momentum, energy, and species concentration at each cell. The variables were stored in a staggered fashion where they made more physical sense for cell conservation. For each cell, the velocity components were stored at downstream boundaries, whereas all pressures and temperatures were stored at the cell center. The hybrid difference scheme demonstrated by Patankar (ref.12) was used to preserve the relative contribution of convection and diffusion to a cell from its neighbor in terms of cell Peclet number. The discretized equations were solved by using the SIMPLEST algorithm (ref.13). The convergence of the numerical solution was monitored by spot checking of field values during the course of the computation and by calculating and monitoring the sum of residuals for each equation. Iterations were continued until sum of residuals for each computational cell dropped below  $10^{-7}$ . All equations had to be solved simultaneously because of the coupling of velocity, temperature, and concentration through the buoyancy terms.

## RESULTS AND DISCUSSION

The numerical solution procedure described in the last section was used to compute the velocity components, and temperature and concentration distributions for different combinations of Reynolds number, Richardson number ( $Ri$  and  $Ri^*$ ), Prandtl number, and Schmidt number. These results were used to predict Nusselt and Sherwood numbers which quantified the rates of heat and mass transfer. Figure 2 shows the variation of the vertical component of velocity across the thickness of the boundary layer for a combination of  $Re = 10^3$ ,  $Ri = 1$ ,  $Ri^* = 0$ , and  $Pr = 0.7$ . Physically, it corresponds to pure heat transfer from an isothermal vertical plate to air. The plot shows the velocity profile at four different locations on the plate. Of these four locations chosen, two were near the leading edge and the other two farther downstream (looking at both natural convection and forced flow directions). These were chosen to observe the increasing influence of the boundary layer growth. It is observed that, at all four locations, the vertical component of velocity has a bell shaped structure typical for natural convection with zero velocity at the wall as well as at the edge of the boundary layer. For any given value of  $Z$  (horizontal location), the magnitude of  $V$  increases with increasing  $Y$  (vertical location). This is because of the growth of buoyancy-induced boundary layer in the vertical direction of the plate. The effects of buoyancy becomes stronger with increase in vertical height. For any given  $Y$ , there is a very significant increase of buoyant flow with increase in the horizontal coordinate. The forced convection boundary layer develops in the horizontal direction. The effects of forced flow remains strong near the near edge of this boundary layer. As the fluid particles move downstream, their horizontal component of velocity decreases because of the viscous resistance from the wall. With increase in horizontal location, the effects of forced convection become weaker, and buoyancy becomes the more dominant transport mechanism.

Figure 3 shows the variation of horizontal component of velocity across the boundary layer. As expected, the horizontal component of velocity increases monotonically from zero to the free stream value with increase in  $X$  at locations on the plate. It may be noticed that at smaller values of  $Z$ , there is no significant change of  $W$ -velocity profile with vertical distance. This is because buoyancy is relatively weaker in that region. Further downstream in the horizontal direction, the magnitude of  $W$ -velocity decreases with  $Y$  because of a significant increase in buoyancy induced flow. The continuity has to be preserved at all locations of the flow. Therefore, a steeper variation of one velocity component results in a corresponding variation in the other velocity component. The distribution of temperature across the thickness of the boundary layer is demonstrated in Figure 4 for the same combination of parameters used in figures 2 and 3. Analogous to a two-dimensional boundary layer flow (for either natural or forced convection), the temperature decreases monotonically with  $X$  at all locations on the plate. The slope of the temperature curve at the wall is proportional to the rate of heat transfer from the wall. It may be noticed that heat transfer is larger near both forced and natural convection leading edges and increases as the boundary layer increases in thickness. Comparing with figure 3, it can be noticed that the thickness of the thermal boundary layer is somewhat larger because of the Prandtl number smaller than 1.

The effects of Reynolds and Prandtl number on the flow and heat transfer are demonstrated in figures 5 and 6. Figure 5 shows the variation of the vertical component of velocity across the boundary layer for a given plate location, for a number of combinations of Reynolds and Prandtl number. The corresponding plots for temperature distribution are shown in figure 6. It can be noticed that with increase in Reynolds number, the thickness of both velocity and thermal boundary layer decrease. The decrease in boundary layer thickness causes a slight increase for the peak of the vertical velocity even though the Richardson number is preserved constant. With increase in Reynolds number, the slope of the temperature curve at the wall also increases. This indicates a larger rate of heat transfer. The increase of heat transfer with fluid velocity is obviously expected. With increase of Prandtl number, both vertical component of velocity and boundary layer thickness decrease. The temperature curve becomes steeper showing an increase of heat transfer rate with Prandtl number.

The effects of the variation of Richardson number ( $Ri$ ) is explored in figures 7 and 8. Richardson number indicates the ratio of buoyant force and the inertia due to forced convection. The usual definition of Richardson number is modified in the present study with the plate aspect ratio to account for different lengths and heights of the plate. For a given Reynolds number and aspect ratio, a higher Richardson number ( $Ri$ ) implies a higher Grashof number ( $Gr_H$ ), which in turn means a stronger natural convection component and smaller boundary layer thickness. This can be clearly seen in figure 7 where the vertical component of velocity is plotted for a number of combinations of Reynolds and Prandtl number. Comparing the peak values of  $V$ , it can be realized that a ten time increase in  $Ri$  results in more than 3 times increase in vertical velocity. Results for both Prandtl numbers confirm the same trend, but a larger Prandtl number results in a smaller boundary layer thickness and a smaller vertical velocity. In figure 8, it can be noticed that the temperature curve becomes steeper and the rate of heat transfer at the wall increases with increase in both Reynolds and Prandtl numbers.

The distribution of Nusselt number over the plate is demonstrated in figure 9, where the variation of Nusselt number with the horizontal coordinate is plotted for two different vertical locations. Results for both fluid systems ( $Pr=0.7$  and  $7$ ) are shown in the figure. The Nusselt number is calculated here with the vertical height as the length scale. The plot therefore essentially demonstrates the variation of the actual heat transfer coefficient. In a cross-flow situation, both vertical and horizontal distances are useful length scales and can be used in the calculation of dimensionless parameters. The Nusselt number is maximum near the vertical leading edge, drops down very rapidly as one proceeds along  $Z$  and finally reaches a stable value at large values of  $Z$ . The magnitude of  $Nu$  for any given Reynolds number and vertical location is significantly higher for an higher Prandtl number. This is because of the smaller boundary layer thickness and steeper temperature profile at the wall. The effects of Reynolds number (strength of the forced flow) on Nusselt number is shown in figure 10. It can be noticed that the increase of Nusselt number with Reynolds number is very significant at all locations on the plate. Therefore, a reasonable cross-flow may very significantly alter the fluid flow and heat transfer scenario in an otherwise natural convection situation. Comparing with the magnitude of Nusselt number for pure natural convection flow, it was noticed that an order of magnitude increase in heat transfer was noticed at smaller  $Z$ -locations. The enhancement factor became smaller at larger values of horizontal coordinate.

Mass transfer from a vertical plate in the presence of a horizontal cross-flow was studied for two specific fluid systems. These are: the evaporation of water from a porous vertical wall which involves the diffusion of water vapor to ambient air; and the dissolution of sodium chloride into water. The Schmidt number for these diffusion processes under normal atmospheric pressure and temperature are  $0.6$  and  $580$ , respectively. To illuminate the mass transfer process, the vertical wall containing the diffusing medium is assumed to be at the same temperature as the free stream. In addition Soret and Dufor effects are neglected. Therefore, Richardson number for heat transfer ( $Ri$ ) is zero during these mass transfer processes. The buoyant force is created due to concentration difference and the corresponding Richardson number is labeled as  $Ri^*$ .

The variation of the vertical fluid velocity and the concentration of water vapor into air are shown in figures 11 and 12 for different locations of the plate. It is not surprising that the  $V$  distribution looks very similar to that in figure 2 and concentration distribution looks similar to that of temperature distribution presented in figure 3. This is because, in either case though the cause of the buoyancy force is different, the resulting effect is almost the same. Also, we are considering the case of  $Ri^*=1$ , which means that the buoyancy forces are about the same order of magnitude of the forced flow. Hence, even though the physics of the problem is totally different for heat transfer and for mass transfer, mathematically they are very similar. For locations near the vertical leading edge (smaller  $Z$ ), forced convective flow predominates and there is not much change in the  $V$  or  $T$  profiles with  $Y$ . But as one proceeds further downstream, the natural convective effects begin to show up and the magnitude of the peak value of  $V$  increases. From figure 12, it can be seen that the concentration gradient is higher at

locations nearer the leading edge, thus implying that the rate of mass transfer is higher here.

The effects of Reynolds number on the vertical velocity and concentration profiles for a particular location in the plate is shown in figures 13 and 14. A larger Reynolds number decreases the boundary layer thickness and increases the slope of the concentration curve. Therefore, the rate of mass transfer increases. The effect of Schmidt number is very significant. It significantly enhances the rate of mass transfer. The vertical velocity for the dissolution of NaCl into water is much smaller in magnitude compared to the vertical velocity attained during diffusion of water vapor into air. The vertical velocity,  $V$  increases greatly with increase in  $Ri^*$  (figure 15). This is due to the fact that for any given values of Reynolds number and any aspect ratio of the plate,  $Ri^*$  is directly proportional to  $Gr_H^*$ , which controls the buoyancy force. Increase in  $Ri^*$  causes reduction of the thermal boundary layer thickness and results in steeper concentration profiles, suggesting a high diffusion rate of the species. Comparing the two fluid systems, the rate of mass transfer is larger for NaCl-H<sub>2</sub>O system owing to much steeper concentration profile at the wall.

The Sherwood number ( $Sh$ ) variation along the  $Z$  direction is plotted in figure 17 for different  $Y$ -locations for a fixed  $Re$  and  $Ri^*$ . Results for both flow systems has been shown in this plot. Analogous to heat transfer, the mass transfer rate is largest near the leading edge for forced convection, diminishes monotonically with  $Z$ , and approaches a constant value at locations far away from the leading edge. The Sherwood number is higher for higher values of  $Y$  and increases significantly with  $Sc$ , thus stressing the importance of fluid properties in determining the mass transfer coefficient. The variation of  $Sh$  along the  $Z$ -direction for different values of  $Re$ , for  $Sc=0.6$  and  $Sc=580$  is shown in figure 18. It can be seen that increase in Reynolds number increases  $Sh$  significantly. This effect is more pronounced at locations near the forced convective leading edge. Therefore, the presence of a cross-flow may very significantly enhance the rate of mass transfer in practical diffusion processes.

## CONCLUSIONS

The objective of the present analysis was to identify the relative importance of the free and forced mode of transport at different locations over a vertical flat plate in cross-flow and also to determine the influence of the different dimensionless parameters on the flow structure and on the rate of heat and mass transfer. It was found that forced convection dominates at locations near the vertical leading edge and natural convection attains importance at locations further downstream. The heat as well as mass transfer coefficients are higher at the leading edge owing to smaller thermal boundary layer thickness and steeper gradients of temperature and concentration. With increase in Reynolds number and/or Prandtl number, the boundary layer thickness became smaller and both heat and mass transfer coefficient increased. A larger Richardson number ( $Ri$  or  $Ri^*$ ) resulted in larger buoyancy-induced transport. The combined effects of natural and forced convection resulted in much larger overall rate of heat and mass transfer.

## NOMENCLATURE

A	Aspect ratio, ratio of the length of the plate to its height ( $L/H$ )
C	Mass concentration
D	Mass diffusivity
g	Acceleration due to gravity
G	Mass transfer coefficient
$Gr_H$	Grashof number for heat transfer, $g\beta H^3 (T_w - T_\infty)/\nu^2$
$Gr_H^*$	Grashof number for mass transfer, $g\beta^* H^3 (C_0 - C_\infty)/\nu^2$

h	Heat transfer coefficient
H	Height of the plate ( in the y-direction )
k	Thermal conductivity
L	Length of the plate ( in the z-direction )
Nu	Nusselt number, $hy/k$
Pr	Prandtl number
Re	Reynolds number, $w_{\infty}L/\nu$
Ri	Richardson number for heat transfer, $Gr_H A^3 / Re^2$
Ri*	Richardson number for mass transfer, $Gr_H^* A^3 / Re^2$
Sc	Schmidt number
Sh	Sherwood number, $Gy/\rho D$
T	Temperature
u	Velocity component in the x-direction
U	Dimensionless velocity component in the x-direction, $u/w_{\infty}$
v	Velocity component in the y-direction
V	Dimensionless velocity component in the y-direction, $v/w_{\infty}$
w	Velocity component in the z-direction
W	Dimensionless velocity component in the z-direction, $w/w_{\infty}$
x	Normal coordinate
X	Dimensionless normal coordinate, $x/L$
y	Vertical coordinate
Y	Dimensionless vertical coordinate, $y/L$
z	Horizontal coordinate
Z	Dimensionless horizontal coordinate, $z/L$

#### Greek Symbols

$\alpha$	Thermal diffusivity
$\beta$	Coefficient of thermal expansion
$\beta^*$	Volume expansion coefficient for concentration
$\nu$	Kinematic viscosity
$\theta$	Dimensionless temperature, $(T - T_{\infty}) / (T_0 - T_{\infty})$
$\psi$	Dimensionless concentration, $(C - C_{\infty}) / (C_0 - C_{\infty})$
$\rho$	Density

#### Subscripts

0	Plate-fluid interface
-	Free-stream condition

#### REFERENCES

1. Lin, H.T.; Wu, K.Y.; and Hoh, H.L.: Mixed Convection from an Isothermal Horizontal Plate Moving in Parallel or Reversely to a Free Stream. Int. J. Heat Mass Transfer., vol.36, no.14,1993, pp. 3547-3554.

2. Khouaja, H.; Chen, T.S., and Armaly, B.F.: Mixed Convection Along Slender Vertical Cylinders with Variable Surface Heat Flux. *Int. J. Heat Mass Transfer.*, vol.34, no.1, 1991, pp. 315-319.
3. Wickern, G.: Mixed Convection From an Arbitrarily Inclined Semi-Infinite Flat Plate. *Int. J. Heat Mass Transfer.*, vol.34, 1991, pp. 1935-1957.
4. Young, R.J.; and Yang, K.T.: Effect of Small Cross-Flow and Surface Temperature Variation of Laminar Free Convection Along a Vertical Plate., *ASME J. of Applied Mechanics*, vol. 30, 1963, pp. 252-256.
5. Eichhorn, R.; and Hasan, M.M.: Mixed Convection About a Vertical Surface in Cross-Flow: A Similarity Solution., *ASME J. of Heat Transfer*, vol. 102, 1980, pp. 775-777.
6. Plumb, O.A.: The Effect of Crossflow on Natural Convection from Vertical Heated Surfaces. ASME paper no. 80-HT-71, 1980.
7. Evans, G.H.; and Plumb, O.A.: Laminar Mixed Convection from a Vertical Heated Surface in a Cross-Flow. *ASME J. of Heat Transfer.*, vol.104, 1982, pp. 554-558.
8. Evans, G.H.; and Plumb, O.A.: Numerical and Approximate Numerical Solution to a Three-Dimensional Mixed Convection Boundary Layer Flow. *Numerical Heat Transfer*, vol. 5, 1982, pp. 287-298.
9. Keller, H.B.; Cebeci, T.: *Accurate Numerical Methods for Boundary Layers, I. Two-Dimensional Laminar Flows.* Proc. 2nd Int. Conference on Numerical Methods in Fluid Dynamics., Lecture Notes in Physics, vol. 8, Springer-Verlag, New York, 1971.
10. Rahman, M.M.; and Carey, V.P.: Transient Cross-Flow Mixed Convection Adjacent to an Isothermal Vertical Plate in Air. Proc. 8th Int. Heat Transfer Conf., San Fransisco, vol. 3, 1986, pp. 1439-1444.
11. Rahman, M.M.; and Carey, V.P.: Steady and Transient Mixed Convection Near a Vertical Uniformly Heated Surface Exposed to Horizontal Fluid Flow. *Numerical Heat Transfer*, vol. 19, 1986, pp. 327-347.
12. Patankar, S.V.: *Numerical Heat Transfer and Fluid Flow.* Hemisphere Publishing, Washington, D.C., 1980.
13. Spalding, D.B.: *Mathematical Modeling of Fluid Mechanics, Heat Transfer and Chemical Reaction Processes.* A Lecture Course, CFDU Report, HTS/80/1, Imperial College, London, 1980.

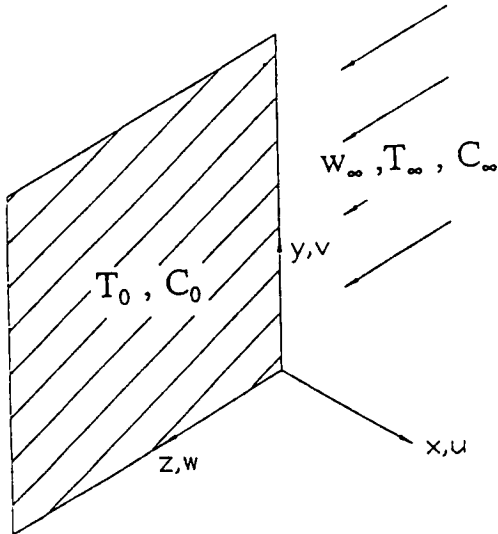


Figure 1. Schematic of the physical problem

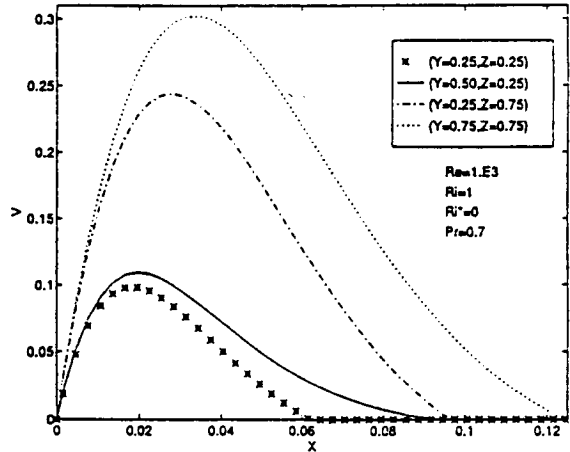


Figure 2. Vertical velocity profile at different locations on the plate

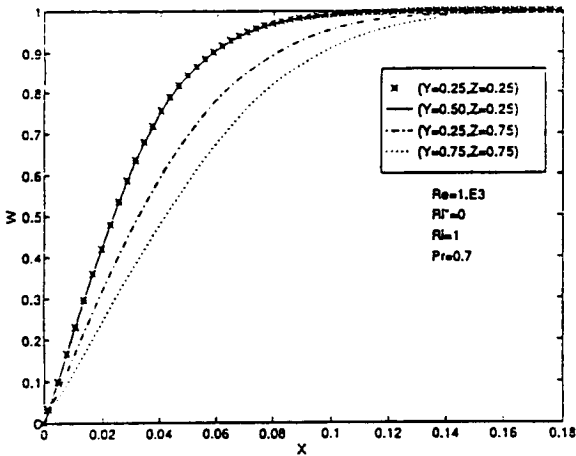


Figure 3. Horizontal velocity profile at different locations on the plate

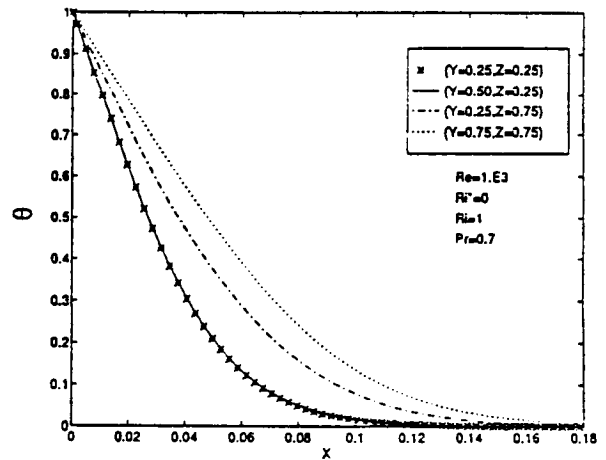


Figure 4. Temperature distribution at different locations on the plate

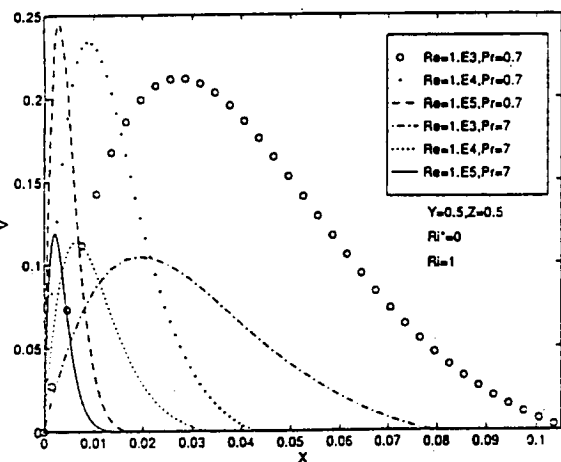


Figure 5. Vertical velocity profile at different Reynolds number

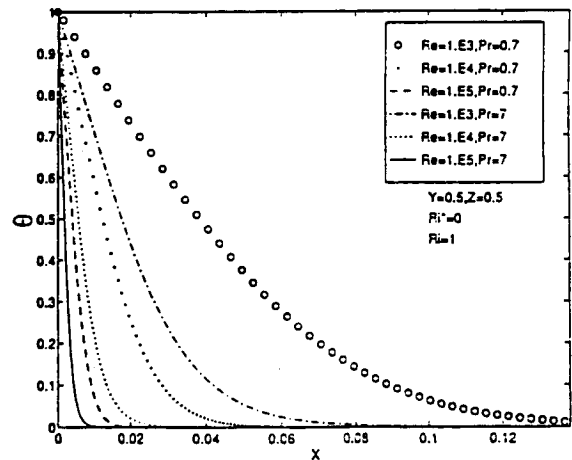


Figure 6. Temperature distribution at different Reynolds number

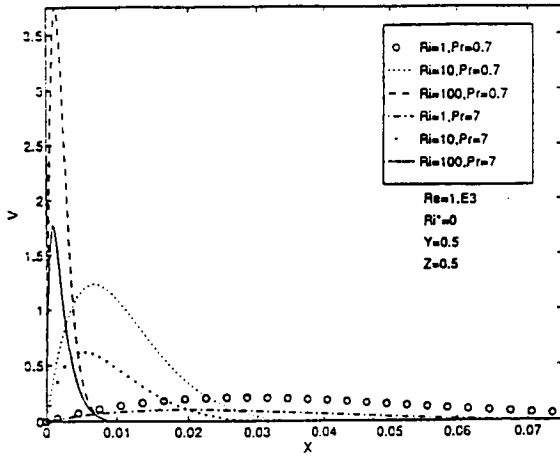


Figure 7. Vertical velocity profile at different Richardson number

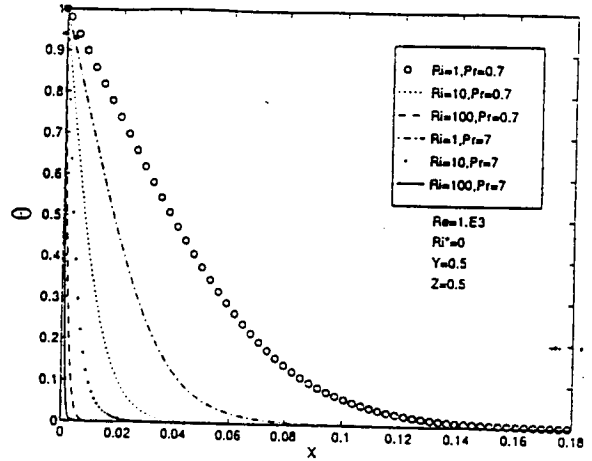


Figure 8. Temperature distribution at different Richardson number

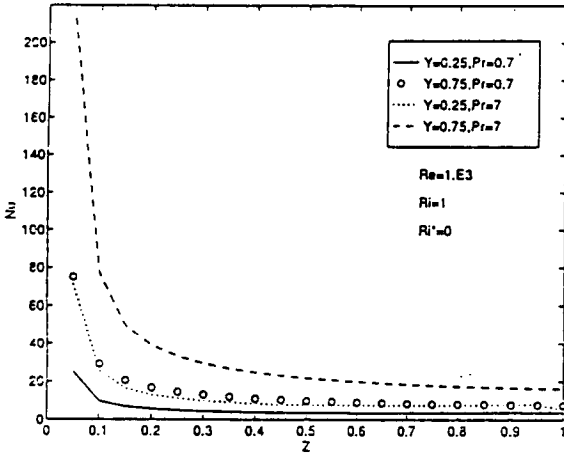


Figure 9. Nusselt number variation over the plate

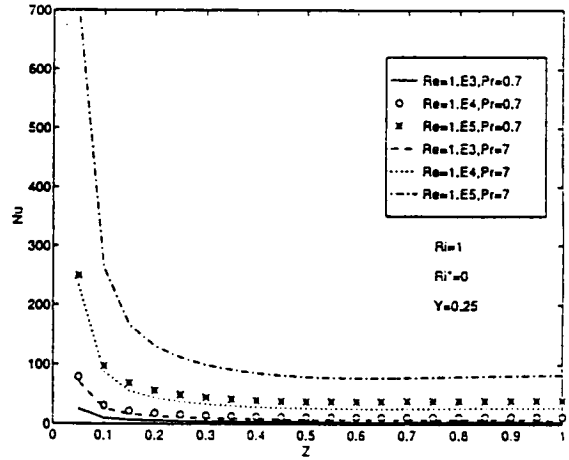


Figure 10. Nusselt number variation at different Reynolds number

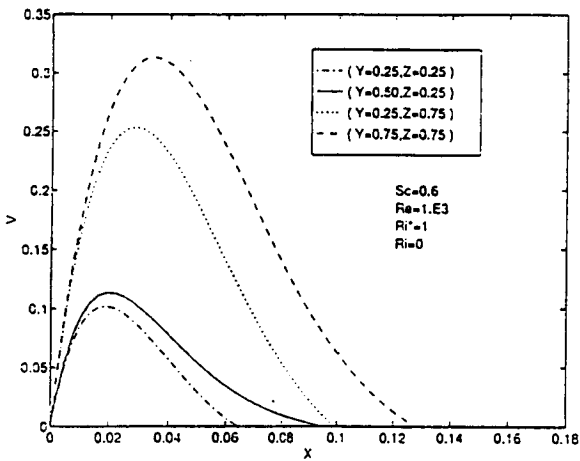


Figure 11. Vertical velocity profile at different locations on the plate

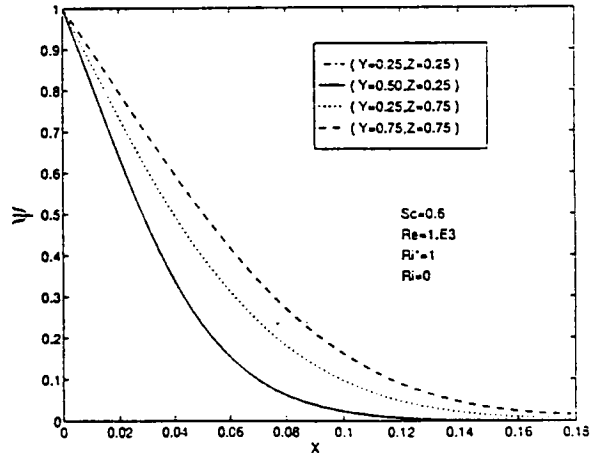


Figure 12. Concentration distribution at different locations on the plate

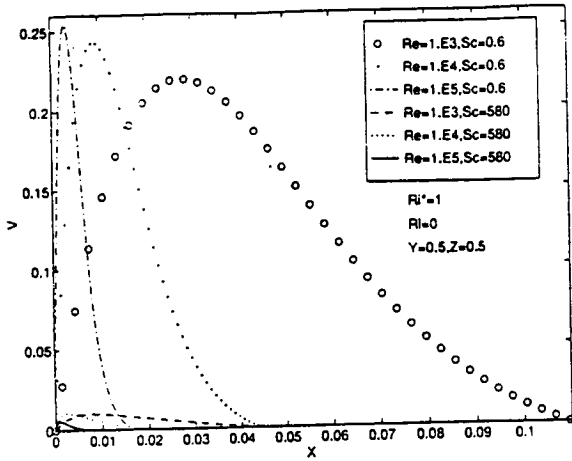


Figure 13. Vertical velocity profile at different Reynolds number

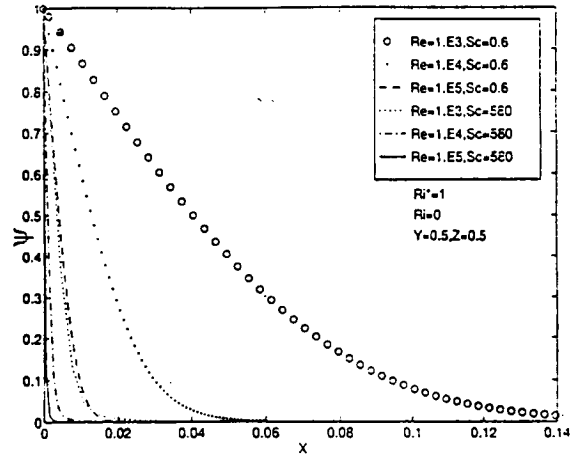


Figure 14. Concentration distribution at different Reynolds number

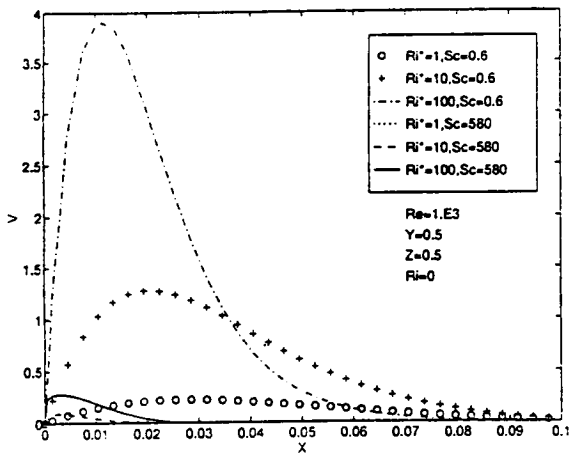


Figure 15. Vertical velocity profile at different Richardson number

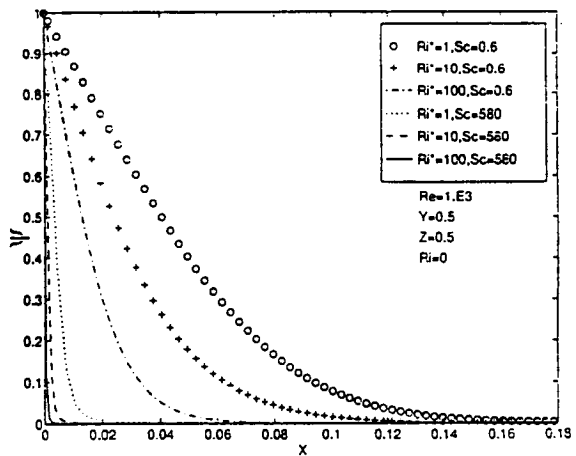


Figure 16. Concentration distribution at different Richardson number

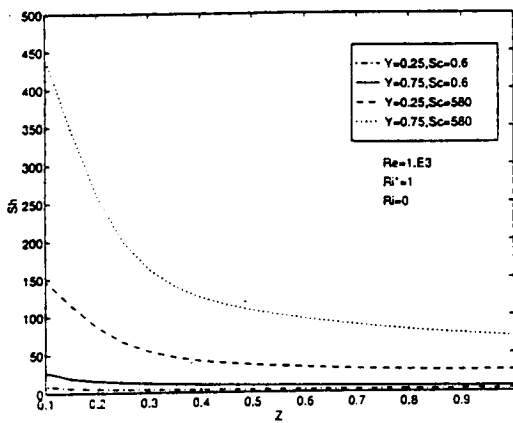


Figure 17. Sherwood number variation over the plate

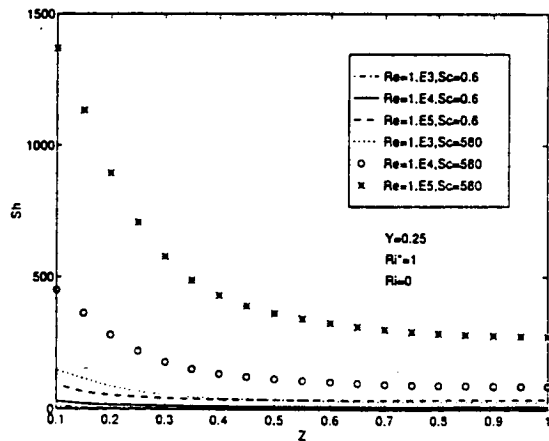


Figure 18. Sherwood number variation at different Reynolds number